Direct evidence of causality between chemical purity and band-edge potential fluctuations in nanoparticle ink-based $Cu_2ZnSn(S,Se)_4$ solar cells

S. Campbell[a], Y. Qu[a], J. Major[b], D. Lagarde[c], C. Labbé[d], P. Maiello[a], V. Barrioz[a], N. S. Beattie[a], G. Zoppi[a,*]

[a]*Department of Mathematics, Physics and Electrical Engineering, Ellison Building, Northumbria University, Newcastle upon Tyne, NE1 8ST, UK*
[b]*Stephenson Institute for Renewable Energy, University of Liverpool, Liverpool L69 7ZF, UK*
[c]*Institut National des Sciences Appliquées, 135 Avenue de Rangueil, 31077 Toulouse Cedex 4, France*
[d]*École nationale supérieure d'ingénieurs de Caen, 6 boulevard Maréchal Juin CS45053, 14000 Caen, France*

Abstract

Kesterite solar cells based on chalcogenide $Cu_2ZnSn(S,Se)_4$ (CZTSSe) are a viable approach to thin film photovoltaics, utilising Earth-abundant, non-toxic elements. CZTSSe films produced from nanoparticle inks offer a cost-effective solution-based method of fabrication. However, improving efficiency in these devices has proved challenging, in part due to the presence of detrimental complex defects within the bulk of the CZTSSe absorber. In this study, the behaviour of nanoparticle-based CZTSSe absorbers and solar cells

*Corresponding author
Email addresses: s.campbell@northumbria.ac.uk (S. Campbell), y.qu@northumbria.ac.uk (Y. Qu), Jon.Major@liverpool.ac.uk (J. Major), delphine.lagarde@insa-toulouse.fr (D. Lagarde), christophe.labbe@ensicaen.fr (C. Labbé), p.maiello@northumbria.ac.uk (P. Maiello), vincent.barrioz@northumbria.ac.uk (V. Barrioz), neil.beattie@northumbria.ac.uk (N. S. Beattie), guillaume.zoppi@northumbria.ac.uk (G. Zoppi)

made from relatively low and high quality grade chemicals is investigated with a view to improving cost-effectiveness of the ink-based fabrication process. Photoluminescence (PL) spectroscopy revealed the presence of similar shallow acceptor plus shallow donor states in both low and high purity precursor absorbers. We demonstrate a relationship between the average depth of energy band-edge potential fluctuations and absorber quality where the higher grade chemical precursor-based absorber outperforms the lower purity version. In addition, the low purity precursor absorber had a higher total defect density resulting in a 10 meV increase in the average electrostatic potential fluctuations. Deep level transient spectroscopy (DLTS) in solar devices indicated the presence of detrimental deep defect states in both types of absorber. Notwithstanding the high purity precursor absorber with lower defect density, the power conversion efficiencies of both types of CZTSSe solar cells were similar ($\sim$5%), implying an issue other than defects in the absorber bulk inhibits device performance as evidenced by quantum efficiency analysis and current-voltage measurements.

Keywords: $Cu_2ZnSn(S,Se)_4$ (CZTSSe), Thin film solar cells, Photoluminescence (PL), Deep Level Transient Spectroscopy (DLTS), Defects

1. Introduction

In recent years, the impetus to fabricate low-cost thin-film photovoltaics from naturally abundant, non-toxic elements has focused research interest on copper-based quaternary chalcogenide kesterites, such as Cu_2ZnSnS_4 (CZTS), $Cu_2ZnSnSe_4$ (CZTSe) and $Cu_2ZnSn(S_xSe_{1-x})$ (CZTSSe) (Kumar et al., 2015; Liu et al., 2016). These materials offer a more sustainable alternative to the current commercially-available thin-film solar cell absorbers CdTe and $CuIn_yGa_{1-y}Se_2$ (CIGS). They are direct bandgap semiconductors with high absorption coefficients in the visible range (α >10^4 cm^{-3}) and CZTSSe has the additional benefit of a tunable bandgap dependent on the S/Se ratio (1.0 eV, x=1 to 1.5 eV, x=0) (He et al., 2012; Siebentritt and Schorr, 2012). Despite a single junction CZTSSe solar cell having a theoretical Shockley-Queisser maximum efficiency limit of 32.2%, polycrystalline CZTSSe devices using a solution approach with reactive hydrazine as the solvent, have only attained a power conversion efficiency (PCE) of 12.6% (Wang et al., 2013). A less hazardous strategem based on CZTS nanoparticle inks annealed in the presence of Se has achieved device efficiency approaching 10% (Hages et al., 2016). Polycrystalline thin-film solar cells are inherently susceptible to the formation of mid-gap defects, which act as electron traps within the bulk of the absorber, and defects at the buffer-absorber interface which inhibit charge transport. Due to the complexity of the pentanary kesterite crystal structure, a variety of intrinsic lattice defects can form which influence the optical and electronic properties of the CZTSSe absorber (Chen et al., 2013). Density functional theory and first principle calculations have been employed to identify a number of intrinsic defects in bulk CZTSSe,

which range from charged point defects such as elemental vacancies, anti-sites and interstitials to neutral defect complexes. Some defects, like shallow acceptors $V_{Cu}{}^{-}$ and $Cu_{Zn}{}^{-}$, are beneficial and are responsible for the p-type conductivity of the absorber. Conversely, deleterious defects such as deep donor antisites $Sn_{Cu}{}^{3+}$ and $Sn_{Zn}{}^{2+}$, form mid-gap traps which act as effective electron-hole recombination centres.

Band-tails may also be present within the kesterite bulk which have been suggested as contributing to Shockley-Read-Hall (SRH) recombination (Mendis et al., 2013). Two rudimentary processes are understood to cause band-tailing: i) an elevated concentration of highly-compensated charged defects which result in an electrostatic potential fluctuation of the valence and conduction bands (VB and CB, respectively) and ii) changes in compositional and/or crystalline homogeneity of the absorber, which cause the VB and CB edges to waver, inducing bandgap fluctuations (Gokmen et al., 2013).

In this article we present complementary photoluminescence (PL) and deep level transient spectroscopy (DLTS) studies of nanoparticle-based CZTSSe thin films and devices fabricated from low and high purity precursor chemicals (subsequently referred to as film LP and HP, respectively). The evolution of PL spectra over a range of cryogenic temperatures can be used to elucidate details of shallow defects within both types of CZTSSe absorber, whereas DLTS is used to probe deeper, mid-gap states. Employing both techniques in conjunction provides comprehensive quantitative information on root-mean-square potential fluctuation depths of band egdes (γ), defect activation energies (E_A), defect concentrations (N_t) and defect capture cross-sections (σ_t) of both types of absorber, which is correlated to the structural

quality of the material.

2. Experimental details

Low and high quality grade metallic sources and solvent oleylamine were used for CZTS nanoparticle synthesis to investigate their influence on the absorbers' behaviour and subsequent solar cells' performance. Low and high purity nanoparticle inks were prepared by varying the metallic sources and solvent as listed in Supp. Table S1. CZTS nanoparticles were fabricated using a hot-injection method where a sulphur-OLA solution was injected into a hot metallic precursors-OLA solution (Qu et al., 2014). The resulting nanoparticle inks were deposited on molybdenum substrates via spin coating to form the CZTS precursor thin film with a thickness around 1 μm (Qu et al., 2016*a*). In order to produce efficient absorbing layers, CZTS precursor thin films were then selenised to introduce grain growth, resulting in CZTSSe absorbers with film thickness $\sim$ 1 μm. This process has been described in greater detail in our previous work (Qu et al., 2016*b*). The crystal structure of both types of film is kesterite in nature determined from X-ray diffraction (XRD). The solar cells were subsequently integrated with a configuration of Mo/CZTSSe/CdS/*i*-ZnO/ITO/Ni-Al. The CdS buffer layer ($\sim$ 55 nm) was deposited using a chemical bath process. *i*-ZnO ($\sim$ 35 nm) and ITO (indium tin oxide, $\sim$ 200nm) layers were then deposited by magnetron sputtering to act as the transparent oxide layers. Front contact grids which are composed of Ni ($\sim$ 50 nm) and Al ($\sim$ 1 μm) layers were deposited through a shadow mask by electron beam evaporation. Finally, nine $\sim$ 0.16 cm^2 cells were defined by mechanical scribing on each substrate (Campbell et al., 2018). PL

spectra were measured using a Horiba Jobin Yvon fully automated spectrometer fitted with an InGaAs PMT detector cooled to -30°C to reduce noise. A 532 nm continuous wave diode-pumped solid state (CW-DPSS) laser was used as an excitation source. All PL measurements were performed on selenised absorber layers deposited on Mo coated glass. PL measurements at varying temperatures were performed by placing the sample in a Janis SHI-4-2 closed cycle refrigeration cryostat using compressed He gas coupled with a Lakeshore Model 335 temperature controller. Time-resolved photoluminescence (TRPL) experiments were performed at 6 K using 800 nm 1.5 ps laser pulses generated by a tunable mode-locked Ti:Sa laser with a repetition rate of 80 MHz. The laser beam is focused onto the sample on a $1/e^2$ diameter spot of $\sim$100 μm and an average power of 20 mW. The PL signal is dispersed by a f-6.5 spectrometer and detected by a synchro-scan Hamamatsu streak camera with an overall time resolution of 15 ps. Deep level transient spectroscopy (DLTS) analysis was performed using a PhysTech FT1230 HERA DLTS system. Emission capacitance transients were recorded using reverse and pulse biases of 5 V and 0 V respectively with a pulse duration of 10 ms. Three transient period widths were recorded 19.2 ms, 192 ms and 480 ms with time constants for the transients being determined via Fourier transform analysis (DLFTS) (Weiss and Kassing, 1988). Quality of the diodes was assessed prior to DLTS measurements using capacitance-voltage (C-V) and current density-voltage (J-V) analysis with C-V measurements being used to calculate shallow acceptor concentration N_A. A temperature range of 80-300 K was used however samples showed significant variation in reverse capacitance values above 220 K hence only data $<$ 220 K was analyzed. Solar

cell J-V parameters were measured using an Abet Technologies solar simulator at 1-sun (100 mW/cm^2) illumination equivalent to air mass 1.5 global spectrum with the light power density calibrated using a Si reference cell. External quantum efficiency measurements were performed using a Bentham spectral response system (calibrated using a Si-InGaAs reference cell) under unbiased conditions. C-V parameters were evaluated using an Agilent E4980a LCR meter and a Shimadzu UV-2600 UV-Vis spectrophotometer was used to obtain transmission/reflectiontion data for CZTSSe films on soda-lime glass (SLG).

3. Results and discussion

CZTSSe is considered a highly-doped and highly-compensated semiconductor due to a high defect density such that the average distance s between defects is less than the defect Bohr radius (Shklovskij and Efros, 1984). The defects tend to be charged and a random distribution of these unscreened charged defects results in electrostatic potential fluctuations inducing band tails (Bauknecht et al., 2001). The presence of both donor and acceptor defects within the material bulk infers that the material is also highly-compensated. Electrostatic potential fluctuations manifest as parallel shifts in valence and conduction band (VB and CB) edges with constant bandgap energy E_g (Campbell et al., 2018). The consequential band tails with energy lower than E_g have an exponentially decaying density of states which produce a broad asymmetric PL spectrum at room temperature (Levanyuk and Osipov, 1981). Similarly, bandgap fluctuations in the CZTSSe material may be induced by Cu-Zn disorder in the kesterite lattice structure (Schorr, 2011;

Choubrac et al., 2013), leading to the formation of non-stoichiometric defect complexes such as $[V_{Cu}{}^{-}+Zn_{Cu}{}^{+}]$ and $[Zn_{Sn}{}^{2-}+2Zn_{Cu}{}^{+}]$ (Chen et al., 2013). Slow-cooling at a rate of 10 ^{o}C/hr after the high-temperature annealing stage of CZTSSe absorber fabrication has been shown to promote clusters of ordered and disordered areas suggesting the random distribution of charged antisite defect $Cu_{Zn}{}^{-}$ is reduced (Paris et al., 2014; Schwarz et al., 2013). Consequently, a reduction in local variations of Cu-Zn disorder produces clusters of lower and higher E_g phases which induces potential fluctuations in the VB and CB of the material.

A model describing the defect-related nature of absorption tails caused by electrostatic potential fluctuations has been proposed by Siebentritt et *al.* (Siebentritt et al., 2006). The low energy tail of PL band *I(E)* is fitted to a Gaussian function,

$$I(E) \sim exp\left(-\frac{(E-E_0)^2}{2\gamma^2}\right) \tag{1}$$

where E_0 is the average emission energy with respect to fluctuating potentials. The magnitude of γ is directly related to the total charged radiative and non-radiative defect density N_t (Dirnstorfer et al., 1998). Evaluating γ from PL emission spectra therefore allows the absorber total defect density N_t to be deduced.

Another generally accepted model to describe the behaviour of sub bandgap defects in CZTSSe is the quasi-donor/acceptor-pair (QDAP) model (Yu, 1977; Schumacher et al., 2006) which is fundamentally linked to the electrostatic potential model. In this case, the distribution of radiative donor and acceptor states contributing to the potential fluctuation are governed by

the Coulombic interaction between the charged defect states. The spectral position of the PL band energy maximum E_{PL} is described by (Schumacher et al., 2006),

$$E_{PL} = E_g - (E_D + E_A) + \frac{e^2}{4\pi\epsilon_0\epsilon_r s} \tag{2}$$

where E_D and E_A are the donor and acceptor energy levels within the CB and VB edges, respectively, ϵ_0 is permittivity of vacuum, ϵ_r is relative permittivity (or dielectric constant) and s is the separation distance between donor and acceptor. The QDAP process is subject to caveats: (i) the spatial separation between charged donor and acceptor defects is large enough that the Coulombic interaction between them is negligible and, (ii) all QDAP states are fully occupied when the QDAP PL peak no longer blue-shifts with increasing excitation intensity, indicating maximum Coulombic attraction between defects (Gunawan et al., 2012). At the point of maximum Coulombic attraction (fully occupied QDAP defects), the blue-shift magnitude of QDAP PL peak ΔE is equivalent to the Coulomb potential energy at that point,

$$\Delta E = \frac{e^2}{4\pi\epsilon_0\epsilon_r s} \tag{3}$$

Thus, the average separation distance s between acceptor/donor can be derived from Eq.(3) and QDAP defect density N_D estimated by assuming a uniform distribution of defects within a spherical volume of radius r,

$$r = s = \left(\frac{4\pi N_D}{3}\right)^{-\frac{1}{3}} \tag{4}$$

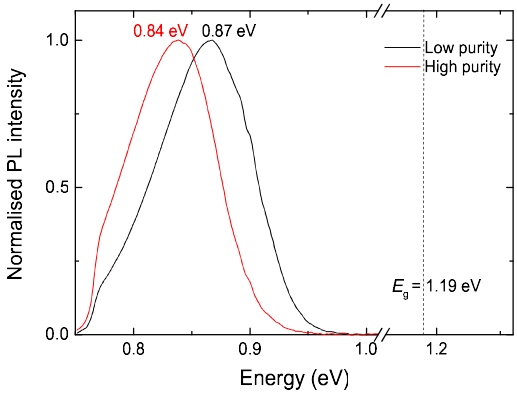

Figure 1: PL of sample LP and HP at 6 K with laser power below PL peak saturation intensity to avoid band-related recombination. The dashed line indicates room temperature bandgap energy E_g of both types of sample.

The normalised 6 K PL spectra of LP and HP films at excitation intensity just below E_{PL} peak saturation are illustrated in Fig. 1. The broad asymmetric shape of the PL bands for both absorbers show a gradual rise in PL intensity on the low energy side and sharper decline on the high energy side of the PL peak, indicating significant band-tailing in the materials. The PL peak maxima are located at 0.86 and 0.84 eV for LP and HP films respectively. The energy peaks are considerably red-shifted from the corresponding room temperature bandgap energy of 1.19 eV, determined from EQE data (discussed later in this section) for both types of absorber. Such a large red-shift could be explained by the presence of deep donor defect Sn_{Zn} with an energy level ∼420 meV below conduction band minima (CBM) or deep acceptor states V_{Sn} or Cu_{Sn} with energy levels ∼400 and 420 meV above valence band maxima (VBM), respectively (Chen et al., 2013). The full

width at half maximum (FWHM) of the PL spectra exhibit a slight decrease from 96 meV for film LP to 92 meV for film HP, with maximum intensity of the PL band of film HP half the intensity of film LP. The low temperature excitation-dependent intensity of the PL spectra for both absorbers is shown in Fig. 2a. The PL band intensity saturates at lower laser power for film HP and a high energy shoulder at ∼0.92 eV emerges upon increasing excitation beyond the threshold intensity (see Supp. Fig. S1). Above the threshold, the lower energy peak red-shifts as the high energy shoulder increases in intensity. Gershon et *al.* observe similar behaviour in CZTS films and state the high energy shoulder is due to a recombination process associated with extended band states and only appears after all localised (QDAP) states are fully saturated (Gershon et al., 2013). This is further evidence QDAP radiative recombination is dominant in the CZTSSe films studied here. The appearance of a high energy shoulder was not observed in the PL bands for film LP, indicating all QDAP states are not occupied. An emperical asymmetric double sigmoidal function was used to fit the PL spectra in order to evaluate the peak maxima at each excitation intensity (Krustok et al., 1999; Yakushev et al., 2017). Both films exhibit a substantial blue-shift of PL peak maxima with increasing laser power until reaching saturation point of PL emission. Fig. 2b shows the evolution of PL band peaks E_{PL} for the CZTSSe samples over a laser intensity range up to the threshold value. Changes in excitation intensity produce a shift in E_{PL} (β) at a rate of β equals 14 and 15 meV/decade and an energy blue-shift magnitude ΔE of 30 and 37 meV for HP and LP films, respectively. Oscillations in the PL bands around 0.9 eV are associated with water vapour absorption of light.

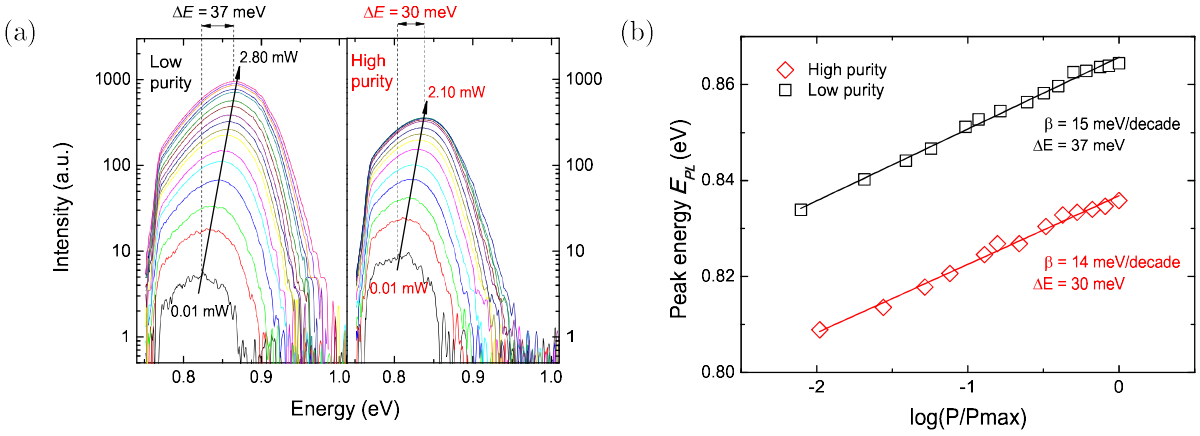

Figure 2: (a) Excitation-dependent PL spectra of sample LP and HP with laser power P up to saturation point of PL emissions together with respective ΔE blue-shift values in $E_P L$ and (b) evolution of PL band maxima with increasing P of LP and HP films with associated shift rates β at 6 K.

Evidence of a significant red-shift in E_{PL} compared to E_g together with large ΔE plus β values for both LP and HP films indicate QDAP defects are predominantly responsible for potential fluctuations in the valence band maxima and conduction band minima (VBM and CBM) of the CZTSSe absorbers. As both films were slow-cooled at a rate of $\sim 7^o$C/min after annealing, it is expected that any bandgap variations contributing to the potential fluctuations should be reduced as the rapid cooling process promotes a more disordered kesterite structure. It is evident that electrostatic potential fluctuations exist in both films with average amplitude γ values of 48.6 and 58.7 meV for films HP and LP respectively which are similar to those previously reported (Gokmen et al., 2013). The QDAP defect density N_D in film LP (2.1 x 10^{18} cm^{-3}) is double that of film HP (1.1 x 10^{18} cm^{-3}) and correlates to a reduction in average defect separation s from 6.0 to 4.8 nm in films HP

and LP respectively. Here, electrons and holes are spatially separated and localised in potential wells within the energy band edges and any radiative recombination requires tunneling of charge carriers from one potential well to another. Increasing the separation distance of the defect centres reduces the probability of radiative emission. The concentration of net (free) charge carriers reduces as the charged QDAP defect density increases. Reducing the density of free carriers lowers the screening effect on the charged defects which, in turn, increases perturbation in the depth of the fluctuating potential γ. The QDAP density is a measure of the shallow donor and acceptor defect concentration responsible for radiative recombination within the material and may not represent the total defect density N_t as the presence of deep and/or non-radiative defects is not accounted for. Therefore the total defect density can be estimated from γ values derived from PL spectra of both films (Dirnstorfer et al., 1998). The optical parameters of LP and HP films are outlined in Table 1.

Temperature dependence of the PL bands was measured at an excitation power slightly lower than the threshold value (at which the high energy shoulder emerges) in order to prevent contributions to PL emissions from band-related transitions. PL spectra of both films over a range of cryogenic temperatures are presented in Fig. 3a. It is apparent that PL emissions are quenched at a lower temperature in film HP and both films exhibit a red-shift in E_{PL} with increasing temperature. The magnitude of the red-shift in E_{PL} (κ) for both types of absorber are shown in Fig. 3b. Initially E_{PL} red-shifts with rising temperature at a similar rate of 0.05 and 0.09 meV/K for films LP and HP respectively. PL emission from film HP is then quenched at a

temperature of ∼100 K, whereas κ increases rapidly above ∼80 K at a rate of 0.84 meV/K in film LP before emissions are finally quenched at ∼140 K. Thermal quenching can be surmised to originate from the thermal depopulation of defect states and/or the activation of non-radiative recombination centres. Similar behaviour was observed by Grossberg et al. in an optical study of defect clusters in CZTS polycrystals (Grossberg et al., 2014). They state the observed evolution of E_{PL} with increasing temperature in CZTS polycrystals followed the temperature dependence of the bandgap energy of the material (Sarswat and Free, 2012). Another study by Yakushev et *al.* revealed comparable temperature trends in PL spectra of CZTSe thin films with varying Cu content (Yakushev et al., 2017).

Table 1: List of optical parameters of low and high purity CZTSSe samples.

	Low purity	High purity	Defect (Chen et al., 2013)
γ (meV)	58.7	48.6	
ΔE (meV)	36.8	29.6	
Defect spacing s (nm)	4.8	6.0	
QDAP density N_D (cm^{-3})	2.1 x 10^{18}	1.1 x 10^{18}	
Defect density N_t (cm^{-3})	2.3 x 10^{19}	1.4 x 10^{19}	
E_a (meV)	(1) 38.3 ± 3.8	(1) 40.1 ± 6.4	V_{Cu}
	(2) 3.2 ± 0.5	(2) 5.9 ± 0.5	Sn_{Cu}

The Varshni equation was used to fit the asymptotic low temperature

behaviour of E_{PL} in both LP and HP films (Varshni, 1967),

$$E_g\left(T\right) = E_g\left(0\right) - \left(\frac{AT^2}{T+B}\right) \tag{5}$$

where *$E_g(0)$* is the bandgap of the semiconductor at 0 K and A, B are fitting parameters specific to the absorber material. Using the fitting parameters extracted from application of the Varshni model, $E_g(0)$ values of 1.24 eV for both films were extrapolated from the room temperature E_g estimate of 1.19 eV. E_{PL} in both films appear to follow the E_g trend at lower temperatures until ~80 K where it deviates markedly in film LP. If electrostatic potential fluctuations of the VBM and CBM are present in the absorbers due to clusters of charged QDAP defects, shallow and deep potential energy wells which follow the fluctuating band edges are formed. Due to a lack of thermal energy at low temperature, carriers are trapped in shallow wells resulting in incomplete occupation of deeper/least energetic wells. As temperature increases the carriers are energised and liberated to fill the deepest wells with a consequent red-shift in E_{PL}. PL emission is quenched in both films due to increasing activation of non-radiative mid-gap recombination centres with rising temperature. The large red-shift in E_{PL} of film LP at temperatures >80 K suggests a different defect is involved in radiative transitions.

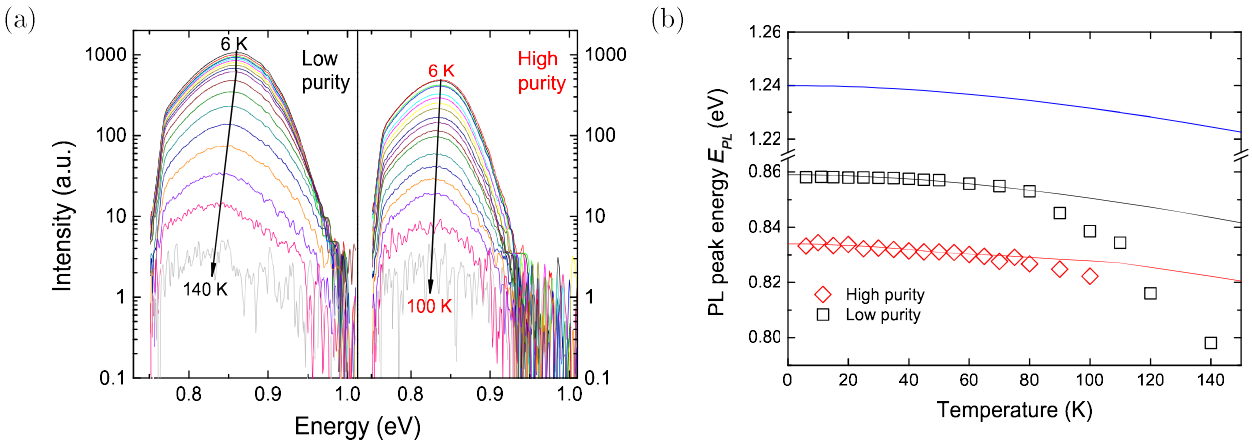

Figure 3: (a) Temperature-dependent PL of sample LP and HP with laser power below PL peak saturation intensity to avoid band-related recombination and (b) evolution of PL band maxima E_{PL} of LP and HP films with increasing temperature. Eq. (5) was used to extrapolate room temperature E_g values to 0 K (blue curve) and temperature-dependent E_{PL} data fitted with same equation (red/black curves).

As temperature increases (up to ~80 K) carriers are ionised and redistributed into other radiative and non-radiative defect states which quench PL emission (T>140 K). Activation energies of the defects involved in radiative recombination can be determined by analysis of the temperature-dependent PL spectra intensity using a two activation energy model proposed by (Luckert et al., 2011),

$$I(T) = \frac{I_0}{1 + C_1 exp\left(-\frac{E_{a1}}{kT}\right) + C_2 exp\left(-\frac{E_{a2}}{kT}\right)} \tag{6}$$

where I_0 is the integrated intensity extrapolated to 0 K, k is the Boltzmann constant, C_1 and C_2 are the process rate parameters and E_{a1} and E_{a2} are the thermal activation energies for the involved defect states. Application of the model to the Arrhenius plots for both films (Fig. 4a) estimated activation

energies of $E_{a1} = 40.1 \pm 6.4$ meV, $E_{a2} = 5.9 \pm 0.5$ meV and $E_{a1} = 38.3 \pm 3.8$ meV, $E_{a2} = 3.2 \pm 0.5$ meV for film HP and LP, respectively. The low activation energies indicate the presence of shallow donor (3-6 meV) and shallow acceptor (38-48 meV) states in both films. A kesterite defect study by Chen et al. would suggest Sn_{Cu} and V_{Cu} are the corresponding donor and acceptor states. They state the Sn 5p electron has a high orbital energy which can be easily ionised, hence the Sn_{Cu} (0/+) defect is located just below the conduction band minimum, which is in agreement with the very shallow donor level observed in both types of absorber (Chen et al., 2013). Also the ionised $V_{Cu}{}^{-}$ defect is the predominant acceptor responsible for p-type conductivity in these CZTSSe absorbers producing a reasonably high concentration of holes (in the region of 10^{15}-10^{16} cm^{-3}). The presence of an additional Sn-related acceptor defect (V_{Sn}, Zn_{Sn} or Cu_{Sn}) could explain the anomalous red-shift in E_{PL} observed in film LP (see Fig. 3b).

The minority carrier dynamics of LP and HP CZTSSe thin films were studied using time-resolved photoluminescence (TRPL) decays, see Fig. 4b. Similar to PL, electron-hole(e-h) pairs are generated, in this case, by a short pulse of incident photons and the time-dependence of the emitted light from recombination of e-h pairs is monitored. The minority carrier lifetime τ is determined from the decay time of charge carrier recombination. In order to evaluate τ, the TRPL decay curves were fitted with a double exponential function (Ohnesorge et al., 1998):

$$I_{PL}(t) = A_1 e^{-\left(\frac{t}{\tau_1}\right)} + A_2 e^{-\left(\frac{t}{\tau_2}\right)} \tag{7}$$

where $I_{PL}(t)$ is the luminescence intensity at time t after the excitation pulse, A_1 and A_2 are are the PL intensities corresponding to the injection regimes

and τ_1 and τ_2 are the fast and slow decay times. The initial fast decay τ_1 can be ascribed to high carrier injection immediately after the excitation pulse and the long tail τ_2 attributed to the minority carrier lifetime of the material (Gunawan et al., 2010; Repins et al., 2012).

Lifetimes of 0.20 and 0.44 ns were observed for films LP and HP, respectively. The lower τ value for film LP would suggest more non-radiative bulk/surface recombination centres are present in the absorber, which is in agreement with the total defect density N_t determined from excitation-dependent PL measurements. Raadik et *al.* propose the shorter carrier lifetime could be related to a higher degree of Cu/Zn disorder in the bulk of the CZTSSe absorber (Raadik et al., 2017). Therefore different recombination processes may be active in LP and HP films. The unexpectedly low carrier lifetime at 6 K observed in this study could be due to high recombination rates at the unpassivated absorber surface.

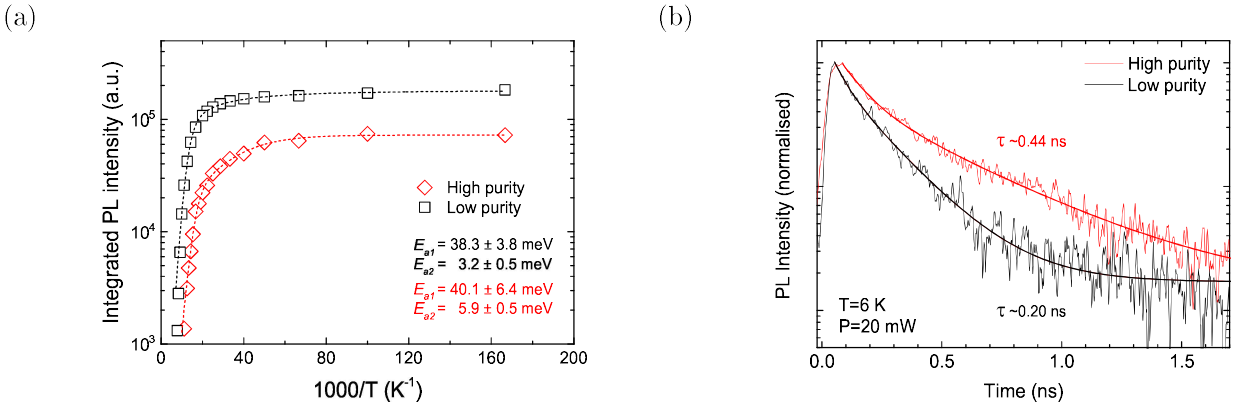

Figure 4: (a) Arrhenius plots of integrated PL intensities and (b) TRPL decays at 6 K for films LP and HP. The solid lines are results of fitting with bi-exponential function.

In order to probe deep defect levels in the CZTSSe devices beyond the

scope of PL spectroscopy, deep level transient spectroscopy (DLTS) is employed to quantify trap activation energies E_T, trap densities N_T and their capture cross-sections σ_T. Supp. Fig. S2 show DLTS spectra for samples LP and HP respectively. In this measurement setup positive ΔC peaks are indicative of hole trap levels with energy values measured with respect to the valence band. Peak positions are analysed over three different transient period widths (19.2 ms, 192 ms, 480 ms) and for a range of correlator functions (Weiss and Kassing, 1988), used to generate Arrhenius plots shown in Fig. 5a. Values for E_T and σ_T are extracted from fitting to the Arrhenius plot whilst the trap density is determined from the magnitude of the capacitance change relative to the reverse bias capacitance (see Table 2).

Table 2: List of electronic parameters of low and high purity CZTSSe samples.

		Trap level E_T (meV)	Capture cross-section σ_T (cm^2)	Trap density N_T (cm^{-3})	Possible defect
Low purity	(1)	86 ± 7	(1.08 ± 0.95) x 10^{-20}	(1.70 ± 0.22) x 10^{14}	Cu_{Zn}
	(2)	167 ± 10	(2.20 ± 1.99) x 10^{-20}	(3.17 ± 0.32) x 10^{13}	Cu_{Sn}, Zn_{Sn}, V_{Sn}
High purity	(1)	87 ± 6	(3.61 ± 1.59) x 10^{-21}	(6.38 ± 0.05) x 10^{14}	Cu_{Zn}

For sample HP a single peak is clearly visible at an energy of $E_T = 87 \pm 6$ meV. The peak is very broad indicating the observed peak may in fact be a distribution of deep levels closely spaced in energy. Attempts were made to separate these levels via a Laplace analysis method (Dobaczewski et al., 2004) however such analysis did not give a definitive answer and was too dependent on the analysis conditions used i.e. number of overlapping transients

permissible. This sample also showed some evidence of a negative peak, indicative of an electron trap, at ∼170 K. On closer inspection, this was found to predominantly occur for short period widths and is in fact measurement artifact related to the recovery time of the capacitance signal. Sample LP showed the same deep level present at $E_T = 86 \pm 9$ meV, although the lower purity sample displayed a slightly lower concentration of this trap level. A second trap state not observable in the HP sample was also observed at an energy of $E_T = 168 \pm 12$ meV but an order of magnitude lower density, 3.17 x 10^{13} cm^{-3}, than for the shallower level . The natural assumption would be that this secondary trap level has arisen as a result of some contaminant within the process solution. It is assumed that the same trap level at 86-87 meV above the VBM in both types of absorber is antisite Cu_{Zn} (Chen et al., 2013). Although the concentration of this defect is higher in device HP than LP, their potentially deleterious effect is mitigated by a lower carrier capture cross-section (σ_{HP} ∼4 x 10^{-21} cm^2 compared to σ_{LP} ∼1 x 10^{-20} cm^2). Ab initio calculations show that the additional defect level in film LP could be Sn-related (V_{Sn}, Cu_{Sn} or Zn_{Sn}) with the likelihood of the defect being Zn_{Sn}, considering the LP absorber is Cu-poor and Zn-rich (see Supp. Table S2). The concentration of any Sn-related defects in film HP should be reduced as the film is compositionally closer to the preferred Cu/(Zn+Sn) ratio of 0.8, see Table 3) (Collord et al., 2015; Fairbrother et al., 2015). CZTSSe films which have low Cu/(Zn+Sn) and high Zn/Sn ratios are predisposed due to the presence of high populations of $[Zn_{Sn}+2Zn_{Cu}]$ charge compensated clusters which are one of the defect complexes responsible for non-stoichiometry in this type of absorber material.

Table 3: Cu/(Zn+Sn) and Zn/Sn ratios of LP and HP thin films and solar cell parameters of subsequently fabricated best devices (with average values in brackets).

	Low purity	High purity
Cu/(Zn+Sn)	0.84	0.82
Zn/Sn	1.07	1.08
V_{OC} (V)	0.31 (0.31)	0.32 (0.32)
J_{SC} (mA/cm^2)	27.2 (26.0)	25.6 (23.7)
FF (%)	59.9 (57.9)	61.9 (56.7)
Efficiency η (%)	5.1 (4.7)	5.1 (4.2)
Carrier lifetime τ (ns)	0.20	0.44
Carrier diffusion length L_d (nm)	203	369

Further studies of the electronic properties of LP and HP solar cells were performed using current density-voltage (J-V), capacitance-voltage (C-V) and external quantum efficiency (EQE) analysis. Fig. 5b shows the J-V plots of the best performing LP and HP devices under 1-sun illumination with the inset showing the average device open circuit voltage V_{OC} and short circuit current density J_{SC}. It is noted that the average V_{OC} of HP cells was slightly higher that that of the LP cells, see inset of Fig. 5b. Conversely, LP devices have a higher J_{SC} value (26.1 mA/cm^2) in comparison to that seen in HP devices (23.7 mA/cm^2). Similar observations were made by Yakushev et *al.* for $Cu_2ZnSnSe_4$ (CZTSe) devices with varying Cu/(Zn+Sn) and Zn/Sn ratios

and were attributed to the degree of Cu-Zn order/disorder in the crystal lattice (Yakushev et al., 2017). EQE plots for LP and HP devices are shown in Fig. 5c, where it can be seen that device LP has enhanced carrier extraction in the wavelength range 600-1000 nm. This anomalous behaviour could be explained by a lower concentration of free charge carriers and will be explored in more detail later in this section. The minority carrier diffusion length L_d for both types of absorber was calculated from EQE measurements in conjunction with optical absorption coefficient α measurements (determined from transmittance/reflectance data, see Supp. Fig. S3) using a method by Courel et *al.* (Courel et al., 2016). It was shown that EQE^{-1} is a linear function of α^{-1} such that:-

$$EQE(\lambda)^{-1} = \frac{1}{(1 - R(\lambda))}\left(1 + \frac{\alpha(\lambda)^{-1}}{L_d}\right) \tag{8}$$

where $R(\lambda)$ is the reflectance of the cell with an intercept on the α^{-1} equal to L_d, see Fig. 5d. Diffusion length values of 203 and 369 nm were determined for LP and HP devices respectively. The reported L_d values are significantly lower than the value of 750 nm observed in the CZTSSe solar cell with record efficiency of 12.6% (Wang et al., 2013). The longer diffusion lengths of carriers in film HP strongly correlates with higher carrier lifetimes measured in CZTSSe bulk. C-V measurements were performed to estimate the depletion region width w and doping density N_A in the CZTSSe absorber layers of devices LP and HP. The inset in Fig. 5d shows the plot of $1/C^2$ versus reverse bias voltage where $<w> = A\varepsilon_0\varepsilon_r/C$ is determined from the measured capacitance value at zero bias and N_A is derived from the slope $d(1/C^2)/dV$. Very short space charge regions widths of 63 and 61 nm were observed for devices LP and HP respectively, with corresponding apparent

doping densities of 2.5 x10^{16} and 3.3 x10^{16} cm^{-3}, in agreement with those observed by Qu et *al.* (Qu et al., 2018). A high doping density is usually associated with a short depletion width in CZTSSe solar cells as $w \propto N_A$ (Ganchev et al., 2011; Haight et al., 2014).

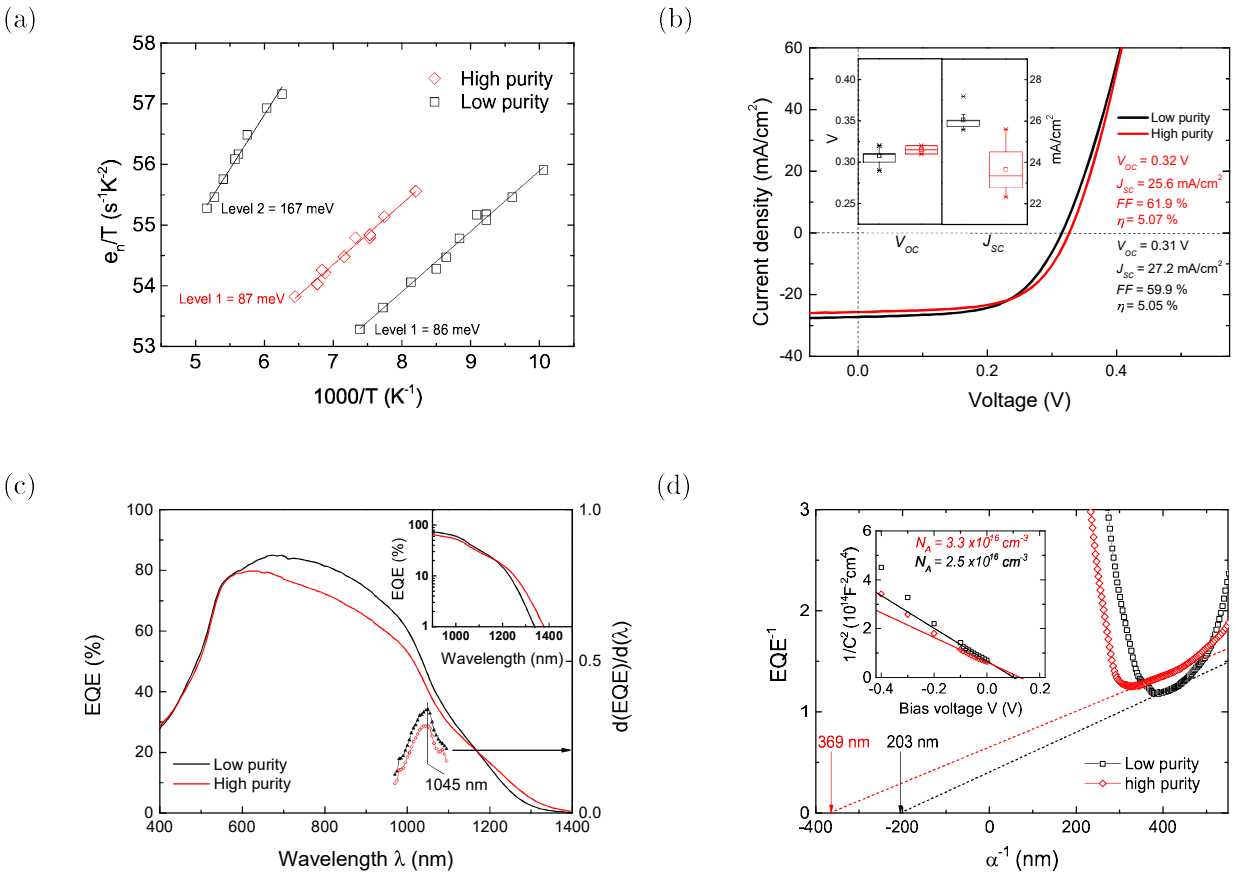

Figure 5: (a) Extracted Arrhenius plots from DLTS spectra, (b) J-V curves of best performing devices with inset showing box plots of average device V_{OC} and J_{SC} parameters, (c) EQE plots with inset showing extended absorption due to tail states in sample HP and (d) calculation of depletion region width w_0 and apparent doping density N_A for samples LP and HP.

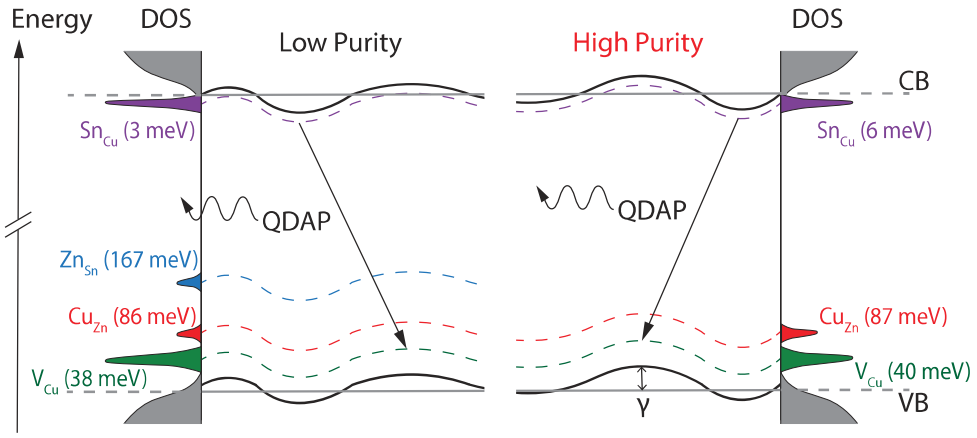

Figure 6: Schematic of electrostatic potential fluctuations in the band edges of LP and HP absorbers with associated defects and densities of state (DOS). The predominant radiative recombination process in both samples involves QDAP defects Sn_{Cu} and V_{Cu}.

Following the selenisation of the CZTS nanoparticle films, EDS compositional analysis of the LP and HP CZTSSe absorbers revealed a greater Cu and Sn loss was observed in LP films, whereas HP films suffered a larger Zn loss. Subsequent Cu/Zn+Sn and Zn/Sn ratios of 0.84, 0.82 and 1.07, 1.08 for respective LP and HP absorbers demonstrate HP films are closer to the preferred CZTSSe composition of Cu/Zn+Sn = 0.8 and Zn/Sn = 1.2 (Collord et al., 2015; Fairbrother et al., 2015). With regard to the elemental losses, it would be reasonable to assume that there could be higher concentrations of Cu- and Sn-related defects in LP films. Recent studies have shown the degree of Cu-Zn order/disorder has a significant impact on the bandgap and crystallinity of CZTSSe absorbers and may be the main cause of bandgap and electrostatic potential fluctuations within the material, as shown in Fig. 6 (Rey et al., 2014; Scragg et al., 2015; Rey et al., 2018; Schorr, 2011).

Considering the small decrease in Cu/Zn+Sn and small increase in Zn/Sn ratios in LP films compared to HP films, higher concentrations of A-type defects ($[V_{Cu}+Zn_{Cu}]$ neutral complexes) may be present in HP films together with higher concentrations of B-type defects ($[Zn_{Sn}+2Zn_{Cu}]$ neutral complexes) in LP films (Lafond et al., 2012; Gurieva et al., 2015). Although the presence of Zn_{Cu} donor defect was not directly observed in either film, their presence can be inferred as high populations of benign $[V_{Cu}+Zn_{Cu}]$ clusters are expected in non-stoichiometric CZTSSe absorbers (Chen et al., 2013).

Perhaps the most interesting observation in this study is the presence of an additional acceptor defect in the LP device located ∼167 meV above the VBM, speculatively attributed to antisite Zn_{Sn}. Chen et *al.* have shown the Zn_{Sn} defect has negligible impact on p-type conductivity but could contribute to luminescence and act as recombination centres (Chen et al., 2013). The presence of radiative Zn_{Sn} defects could explain the increased QDAP density and PL intensity seen in film LP compared to film HP. The significant red-shift of the PL peak in film LP at temperatures greater than 80 K could be attributed to radiative recombination involving the Zn_{Sn} acceptor. The lower QDAP concentration in film HP could also account for quenching of the PL signal at a lower temperature (∼100 K) in this film compared to film LP (∼140 K). It is also possible the anomalous temperture-dependent PL behaviour in film LP could involve Cu_{Zn}-Sn_{Cu} QDAP due to the thermal escape of holes from the shallower V_{Cu} acceptor state to the slightly deeper Cu_{Zn} state, see Fig. 6. According to Chen et *al.* a number of self-compensated defect clusters can be formed in quaternary kesterites. They show the overall formation energy of these defect clusters is significantly decreased relative to

the sum of the individual defects. As the clusters are charge-nuetral and bound by strong Coulomb attraction, their presence should not be detected directly by PL analysis. However, some defect clusters can produce a significant shift in the valence and conduction band edges, effectively reducing the bandgap of the absorber. Large populations of clusters $[2V_{Cu}+Sn_{Zn}]$ or $[2Cu_{Zn}+Sn_{Zn}]$ could exist in both types of absorber given the observed large red-shift of E_{PL} in comparison to the bandgap of the absorbers at 6 K ($\sim$300 meV) which cannot be solely attributed to QDAP defects. The presence of neutral defect clusters would reduce the concentration of shallow acceptor defects which contribute to the overall p-type conductivity of the absorber material. From capacitance-voltage measurements, film LP has a slightly lower apparent doping density N_A in comparison to that of film HP indicating the degree of compensation is greater in this film. The measured concentration of V_{Cu} antisite defects (which are mainly responsible for the p-type conductivity of Cu-poor/Zn- rich CZTSSe films) is around 10^{19} cm^{-3} in both types of absorber whereas both films show $N_A \sim 10^{16}$ cm^{-3} confirming the material is highly compensated.

All optical and electronic parameters indicate films prepared from high purity precursor chemicals are of a higher quality than those fabricated from lower grade materials. However, this improvement in film quality does not translate to an increase in completed device efficiency as both types of device have similar best η values of $\sim$5.1 %. A previous study of CZTSSe solar cells fabricated using the same nanoparticle inks-based method has revealed the devices typically have a contact barrier height of $\sim$40 meV between the CZTSSe absorber and Mo back contact (Campbell et al., 2018). This low

barrier height would suggest the back contact of both types of device is not a factor constraining cell performance and, therefore, attention should be focused on improving buffer/absorber junction and other components in the device architecture.

One important parameter which could be utilised to indicate the quality of CZTSSe absorbers is the mean depth of potential fluctuations γ. Considering a high concentration of Zn_{Sn} defects present in absorber LP (which could contribute to an elevated QDAP density), we see a direct correlation of such QDAP density with γ, suggesting γ is a useful indicator of the presence of specific defects which generate band tails in the material. Yakushev et *al.* observe a similar reduction in γ values when the studied CZTSe films became Cu-poorer and Zn-richer, attributing this change to improved ordering of Cu-Zn atoms within the crystal lattice of the thin film (Yakushev et al., 2017). A similar reduction in γ values are noted in this study. Bourdais et *al.* investigated the effect of Cu-Zn disorder on the V_{OC} deficit in kesterite solar cells also noted that ordering of the CZTSSe absorbers by slow cooling improved the V_{OC} deficit in their devices by 40 meV. Therefore, a reduction in γ value could indicate a reduction in Cu-Zn disorder with an associated increase in V_{OC} (Bourdais et al., 2016). Fig. 6 highlights the main results of the combined optical and electronic studies, principally:

(i) Fluctuations in the band edges of both types of absorber, predominantly caused by variations in electrostatic potential, with an average depth of γ equal to 59 and 49 meV in films LP and HP respectively

(ii) Same shallow donor (Sn_{Cu}) and shallow acceptor (V_{Cu}, Cu_{Zn}) defects present in the bulk of both types of CZTSSe absorber

(iii) Additional deep Sn-related acceptor defect (probably Zn_{Sn}) located 167 meV above the VBM present in sample LP

(iv) Radiative recombination primarily involving QDAP donor Sn_{Cu} and acceptor V_{Cu} defects located 3-6 meV below CBM and 38-40 meV above VBM

(v) V_{Cu} chiefly responsible for p-type conductivity in both types of thin film.

4. Conclusion

In depth optical spectroscopy and electronic studies of CZTSSe absorber layers fabricated from low and high purity precursor chemicals are presented. The high purity chemical recipe produced Cu-poorer and Zn-richer CZTS nanoparticles. Following selenisation of the stacked spin-coated CZTS films, a Zn loss was observed in the HP absorber while a Sn loss was seen in the LP absorber. Comprehensive temperature and excitation dependent analysis of PL spectra together with DLTS enabled identification of shallow and deep defects and QDAP recombination as the predominant recombination mechanism in both types of thin film. The loss of Sn could account for the presence of additional Sn-related defects identified in the LP film. Notwithstanding the improvement in quality of film HP, detailed analysis of the electronic properties of LP and HP solar cells revealed similar performance in both types of device. This implies an underlying issue other than defects in the absorber bulk inhibits device performance which warrants further investigation.

5. Acknowledgements

The authors acknowledge support from the Engineering and Physical Sciences Research Council (EPSRC, Grant EP/N024389/1 and EP/N014057/1) and the North East Centre for Energy Materials (NECEM, Grant EP/R021503/1).

6. References

References

Bauknecht, A., Siebentritt, S., Albert, J. and Lux-Steiner, M. C. (2001), 'Radiative recombination via intrinsic defects in $Cu_xGa_ySe_2$', *Journal of Applied Physics* **89**(8), 4391–4400.

Bourdais, S., Choné, C., Delatouche, B., Jacob, A., Larramona, G., Moisan, C., Lafond, A., Donatini, F., Rey, G. and Siebentritt, S. (2016), 'Is the Cu/Zn Disorder the Main Culprit for the Voltage Deficit in Kesterite Solar Cells?', *Advanced Energy Materials* **6**(12), 1502276.

Campbell, S., Qu, Y., Bowen, L., Chapon, P., Barrioz, V., Beattie, N. and Zoppi, G. (2018), 'Influence of OLA and FA ligands on the optical and electronic properties of $Cu_2ZnSn(S,Se)_4$ thin films and solar cells prepared from nanoparticle inks', *Solar Energy* .

Chen, S., Walsh, A., Gong, X.-G. and Wei, S.-H. (2013), 'Classification of Lattice Defects in the Kesterite Cu_2ZnSnS_4 and $Cu_2ZnSnSe_4$ Earth-Abundant Solar Cell Absorbers', *Advanced Materials* **25**(11), 1522–1539.

Choubrac, L., Paris, M., Lafond, A., Guillot-Deudon, C., Rocquefelte, X. and Jobic, S. (2013), 'Multinuclear (^{67}Zn, ^{119}Sn and ^{65}Cu) NMR spectroscopy an ideal technique to probe the cationic ordering in Cu_2ZnSnS_4 photovoltaic materials', *Physical Chemistry Chemical Physics* **15**(26), 10722.

Collord, A. D., Xin, H. and Hillhouse, H. W. (2015), 'Combinatorial Exploration of the Effects of Intrinsic and Extrinsic Defects in $Cu{-}2ZnSn(S,Se)_4$', *IEEE Journal of Photovoltaics* **5**(1), 288–298.

Courel, M., Valencia-Resendiz, E., Pulgarín-Agudelo, F. and Vigil-Galín, O. (2016), 'Determination of minority carrier diffusion length of sprayed-Cu_2ZnSnS_4 thin films', *Solid-State Electronics* **118**, 1–3.

Dirnstorfer, I., Wagner, M., Hofmann, D., Lampert, M., Karg, F. and Meyer, B. (1998), 'Characterization of CuIn(Ga)Se_2 thin films', *Physica Status Solidi (a)* **168**(1), 163–175.

Dobaczewski, L., Peaker, A. R. and Bonde Nielsen, K. (2004), 'Laplace-transform deep-level spectroscopy: The technique and its applications to the study of point defects in semiconductors', *Journal of Applied Physics* **96**(9), 4689–4728.

Fairbrother, A., Dimitrievska, M., Sánchez, Y., Izquierdo-Roca, V., Pérez-Rodriguez, A. and Saucedo, E. (2015), 'Compositional paradigms in multi-nary compound systems for photovoltaic applications: a case study of kesterites', *Journal of Materials Chemistry A* **3**(18), 9451–9455.

Ganchev, M., Iljina, J., Kaupmees, L., Raadik, T., Volobujeva, O., Mere, A., Altosaar, M., Raudoja, J. and Mellikov, E. (2011), 'Phase composition of selenized $Cu_2ZnSnSe_4$ thin films determined by X-ray diffraction and Raman spectroscopy', *Thin Solid Films* **519**(21), 7394–7398.

Gershon, T., Shin, B., Gokmen, T., Lu, S., Bojarczuk, N. and Guha, S. (2013), 'Relationship between Cu_2ZnSnS_4 quasi donor-acceptor pair density and solar cell efficiency', *Applied Physics Letters* **103**(19), 193903.

Gokmen, T., Gunawan, O., Todorov, T. K. and Mitzi, D. B. (2013), 'Band tailing and efficiency limitation in kesterite solar cells', *Applied Physics*

Letters **103**(10), 103506.
URL: *http://dx.doi.org/10.1063/1.4820250*

Grossberg, M., Raadik, T., Raudoja, J. and Krustok, J. (2014), 'Photoluminescence study of defect clusters in Cu_2ZnSnS_4 polycrystals', *Current Applied Physics* **14**(3), 447–450.

Gunawan, O., Gokmen, T., Warren, C. W., Cohen, J. D., Todorov, T. K., Barkhouse, D. A. R., Bag, S., Tang, J., Shin, B. and Mitzi, D. B. (2012), 'Electronic properties of the $Cu_2ZnSn(Se,S)_4$ absorber layer in solar cells as revealed by admittance spectroscopy and related methods', *Applied Physics Letters* **100**(25), 253905.
URL: *http://dx.doi.org/10.1063/1.4729751*

Gunawan, O., Todorov, T. K. and Mitzi, D. B. (2010), 'Loss mechanisms in hydrazine-processed $Cu_2ZnSn(S,Se_4$ solar cells', *Applied Physics Letters* **97**(23), 233506.
URL: *http://dx.doi.org/10.1063/1.3522884*

Gurieva, G., Dimitrievska, M., Zander, S., Pérez-Rodriguez, A., Izquierdo-Roca, V. and Schorr, S. (2015), 'Structural characterisation of $Cu_{2.04}Zn_{0.91}Sn_{1.05}S_{2.08}Se_{1.92}$', *physica status solidi (c)* **12**(6), 588–591.

Hages, C. J., Koeper, M. J., Miskin, C. K., Brew, K. W. and Agrawal, R. (2016), 'Controlled Grain Growth for High Performance Nanoparticle-Based Kesterite Solar Cells', *Chemistry of Materials* **28**(21), 7703–7714.
URL: *http://dx.doi.org/10.1021/acs.chemmater.6b02733*

583 Haight, R., Shao, X., Wang, W. and Mitzi, D. B. (2014), 'Electronic and
584 elemental properties of the $Cu_2ZnSn(S,Se_4$ surface and grain boundaries',
585 *Applied Physics Letters* **104**(3), 033902.

586 He, J., Sun, L., Chen, S., Chen, Y., Yang, P. and Chu, J. (2012), 'Compo-
587 sition dependence of structure and optical properties of $Cu_2ZnSn(S,Se)_4$
588 solid solutions: An experimental study', *Journal of Alloys and Compounds*
589 **511**(1), 129–132.

590 Krustok, J., Collan, H., Yakushev, M. and Hjelt, K. (1999), 'The role of
591 spatial potential fluctuations in the shape of the PL bands of multinary
592 semiconductor compounds', *Physica Scripta* **T79**(1), 179.

593 Kumar, M., Dubey, A., Adhikari, N., Venkatesan, S. and Qiao, Q.
594 (2015), 'Strategic review of secondary phases, defects and defect-complexes
595 in kesterite CZTS-Se solar cells', *Energy & Environmental Science*
596 **8**(11), 3134–3159.

597 Lafond, A., Choubrac, L., Guillot-Deudon, C., Deniard, P. and Jobic, S.
598 (2012), 'Crystal Structures of Photovoltaic Chalcogenides, an Intricate
599 Puzzle to Solve: the Cases of CIGSe and CZTS materials', *Zeitschrift*
600 *für anorganische und allgemeine Chemie* **638**(15), 2571–2577.

601 Levanyuk, A. P. and Osipov, V. V. (1981), 'Edge luminescence of direct-gap
602 semiconductors', *Soviet Physics Uspekhi* **24**(3), 187–215.

603 Liu, X., Feng, Y., Cui, H., Liu, F., Hao, X., Conibeer, G., Mitzi, D. B. and
604 Green, M. (2016), 'The current status and future prospects of kesterite

605 solar cells: a brief review', *Progress in Photovoltaics: Research and Appli-*
606 *cations* **24**(6), 879–898.

607 Luckert, F., Hamilton, D. I., Yakushev, M. V., Beattie, N. S., Zoppi, G.,
608 Moynihan, M., Forbes, I., Karotki, A. V., Mudryi, A. V. and Grossberg, M.
609 (2011), 'Optical properties of high quality $Cu_2ZnSnSe_4$ thin films', *Applied*
610 *Physics Letters* **99**(6), 062104.
611 **URL:** *http://10.1063/1.3624827*

612 Mendis, B. G., Shannon, M. D., Goodman, M. C. J., Major, J. D., Taylor,
613 A. A., Halliday, D. P. and Durose, K. (2013), 'The nature of electrostatic
614 potential fluctuations in Cu_2ZnSnS_4 and their role on photovoltaic device
615 performance', *Journal of Physics: Conference Series* **471**, 012014.

616 Ohnesorge, B., Weigand, R., Bacher, G., Forchel, A., Riedl, W. and Karg,
617 F. H. (1998), 'Minority-carrier lifetime and efficiency of $Cu(In,Ga)Se_2$ solar
618 cells', *Applied Physics Letters* **73**(9), 1224–1226.

619 Paris, M., Choubrac, L., Lafond, A., Guillot-Deudon, C. and Jobic, S. (2014),
620 'Solid-State NMR and Raman Spectroscopy to Address the Local Structure
621 of Defects and the Tricky Issue of the Cu-Zn Disorder in Cu-Poor, Zn-Rich
622 CZTS Materials', *Inorganic Chemistry* **53**(16), 8646–8653.

623 Qu, Y., Zoppi, G. and Beattie, N. S. (2016*a*), 'The role of nanoparticle
624 inks in determining the performance of solution processed $Cu_2ZnSn(S,Se)_4$
625 thin film solar cells', *Progress in Photovoltaics: Research and Applications*
626 **24**(6), 836–845.
627 **URL:** *http://dx.doi.org/10.1002/pip.2756*

Qu, Y., Zoppi, G. and Beattie, N. S. (2016*b*), 'Selenization kinetics in $Cu_2ZnSn(S,Se)_4$ solar cells prepared from nanoparticle inks', *Solar Energy Materials and Solar Cells* **158**, 130–137.

Qu, Y., Zoppi, G., Miles, R. W. and Beattie, N. S. (2014), 'Influence of reaction conditions on the properties of solution-processed Cu_2ZnSnS_4 nanocrystals', *Materials Research Express* **1**(4), 045040.
URL: *http://dx.doi.org/10.1002/cssc.201600063*

Qu, Y., Zoppi, G., Peter, L. M., Jourdain, S. and Beattie, N. S. (2018), 'Enhanced external quantum efficiency from $Cu_2ZnSn(S,Se)_4$ solar cells prepared from nanoparticle inks', *Japanese Journal of Applied Physics* **57**(8S3), 08RC01.

Raadik, T., Krustok, J., Kauk-Kuusik, M., Timmo, K., Grossberg, M., Ernits, K. and Bleuse, J. (2017), 'Low temperature time resolved photoluminescence in ordered and disordered Cu_2ZnSnS_4 single crystals', *Physica B: Condensed Matter* **508**, 47–50.

Repins, I., Beall, C., Vora, N., DeHart, C., Kuciauskas, D., Dippo, P., To, B., Mann, J., Hsu, W.-C. and Goodrich, A. e. a. (2012), 'Co-evaporated $Cu_2ZnSnSe_4$ films and devices', *Solar Energy Materials and Solar Cells* **101**, 154–159.

Rey, G., Larramona, G., Bourdais, S., Choné, C., Delatouche, B., Jacob, A., Dennler, G. and Siebentritt, S. (2018), 'On the origin of band-tails in kesterite', *Solar Energy Materials and Solar Cells* **179**, 142–151.

650 Rey, G., Redinger, A., Sendler, J., Weiss, T. P., Thevenin, M., Guennou,
651 M., El Adib, B. and Siebentritt, S. (2014), 'The band gap of $Cu_2ZnSnSe_4$:
652 Effect of order-disorder', *Applied Physics Letters* **105**(11), 112106.

653 Sarswat, P. K. and Free, M. L. (2012), 'A study of energy band gap ver-
654 sus temperature for Cu_2ZnSnS_4 thin films', *Physica B: Condensed Matter*
655 **407**(1), 108–111.

656 Schorr, S. (2011), 'The crystal structure of kesterite type compounds A
657 neutron and X-ray diffraction study', *Solar Energy Materials and Solar*
658 *Cells* **95**(6), 1482–1488.

659 Schumacher, S. A., Botha, J. R. and Alberts, V. (2006), 'Photoluminescence
660 study of potential fluctuations in thin layers of $Cu(In_{0.75}Ga_{0.25})(S_ySe_{1-y})_2$',
661 *Journal of Applied Physics* **99**(6), 063508.
662 **URL:** *http://dx.doi.org/10.1063/1.2180429*

663 Schwarz, T., Cojocaru-Mirédin, O., Choi, P., Mousel, M., Redinger, A.,
664 Siebentritt, S. and Raabe, D. (2013), 'Atom probe study of $Cu_2ZnSnSe_4$
665 thin-films prepared by co-evaporation and post-deposition annealing', *Ap-*
666 *plied Physics Letters* **102**(4), 042101.

667 Scragg, J. J. S., Larsen, J. K., Kumar, M., Persson, C., Sendler, J., Sieben-
668 tritt, S. and Platzer Bjorkman, C. (2015), 'Cu-Zn disorder and band gap
669 fluctuations in $Cu_2ZnSn(S,Se)_4$ Theoretical and experimental investiga-
670 tions', *Physica Status Solidi (b)* **253**(2), 247–254.

671 Shklovskij, B. I. and Efros, A. L. (1984), *Electronic properties of doped semi-*
672 *conductors*, Springer.

673 Siebentritt, S., Papathanasiou, N. and Lux-Steiner, M. (2006), 'Potential
674 fluctuations in compensated chalcopyrites', *Physica B: Condensed Matter*
675 **376-377**, 831–833.

676 Siebentritt, S. and Schorr, S. (2012), 'Kesterites-a challenging material for so-
677 lar cells', *Progress in Photovoltaics: Research and Applications* **20**(5), 512–
678 519.

679 Varshni, Y. (1967), 'Temperature dependence of the energy gap in semicon-
680 ductors', *Physica* **34**(1), 149–154.

681 Wang, W., Winkler, M. T., Gunawan, O., Gokmen, T., Todorov, T. K.,
682 Zhu, Y. and Mitzi, D. B. (2013), 'Device Characteristics of CZTSSe
683 Thin-Film Solar Cells with 12.6% Efficiency', *Advanced Energy Materi-*
684 *als* **4**(7), 1301465.

685 Weiss, S. and Kassing, R. (1988), 'Deep Level Transient Fourier Spectroscopy
686 (DLTFS) A technique for the analysis of deep level properties', *Solid-State*
687 *Electronics* **31**(12), 1733–1742.

688 Yakushev, M., Sulimov, M., Márquez-Prieto, J., Forbes, I., Krustok, J., Ed-
689 wards, P., Zhivulko, V., Borodavchenko, O., Mudryi, A. and Martin, R.
690 (2017), 'Influence of the copper content on the optical properties of CZTSe
691 thin films', *Solar Energy Materials and Solar Cells* **168**, 69–77.

692 Yu, P. W. (1977), 'Excitation-dependent emission in Mg-, Be-, Cd-, and
693 Zn-implanted GaAs', *Journal of Applied Physics* **48**(12), 5043–5051.

Appendix A. Supplementary material

Table S1: Chemical composition and concentration details of low/high purity CZTS nanoparticle recipe.

	Low purity recipe		High purity recipe	
Copper(II) acetylacetonate ($Cu(acac)_2$)	97%	*Sigma Aldrich*	99.99%	*Sigma Aldrich*
Zinc acetylacetonate ($Zn(acac)_2$)	*not provided by supplier*	*Alfa Asear*	99.995%	*Sigma Aldrich*
Tin(IV) bis(acetylacetonate) dichloride ($Sn(acac)_2Cl_2$)	95%	*Alfa Asear*	98%	*Sigma Aldrich*
Elemental sulphur (S)	99.98%	*Sigma Aldrich*	99.98%	*Sigma Aldrich*
Oleylamine (OLA)	*technical grade* 70%	*Sigma Aldrich*	98%	*Sigma Aldrich*

Table S2: The composition of precursor and selenised films on bare SLG

Solvent		Cu ($at\%$)	Zn ($at\%$)	Sn ($at\%$)	S ($at\%$)	Se ($at\%$)	$\frac{Cu}{Zn+Sn}$	Zn/Sn	$\frac{Se}{Se+S}$
HP	Precursor	23.93	16.88	14.24	45.95		0.74	1.19	
	Selenised	20.61	13.13	12.12	5.57	48.53	0.82	1.08	0.90
LP	Precursor	23.17	14.3	14.16	48.04		0.80	1.03	
	Selenised	19.09	11.80	11.02	5.02	53.06	0.84	1.07	0.91

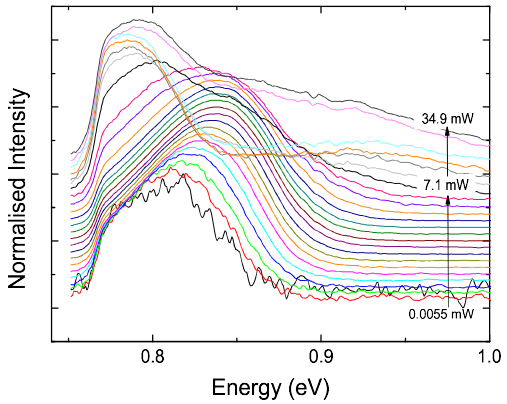

Figure S1: Emergence of high energy 'shoulder' in PL spectra of film HP indicating saturation of QDAP defects and an increasing contribution to PL intensity from band-related radiative recombination.

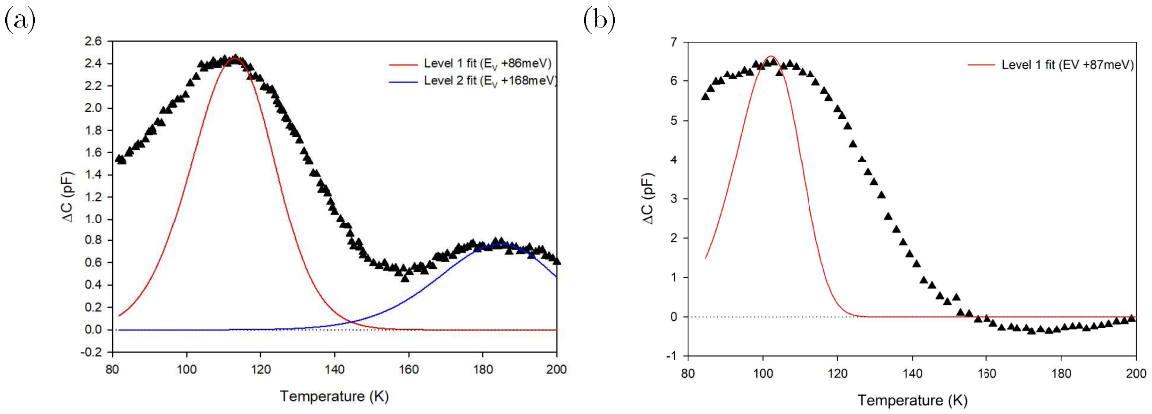

Figure S2: DLTS spectra recorded for (a) sample LP and (b) sample HP.

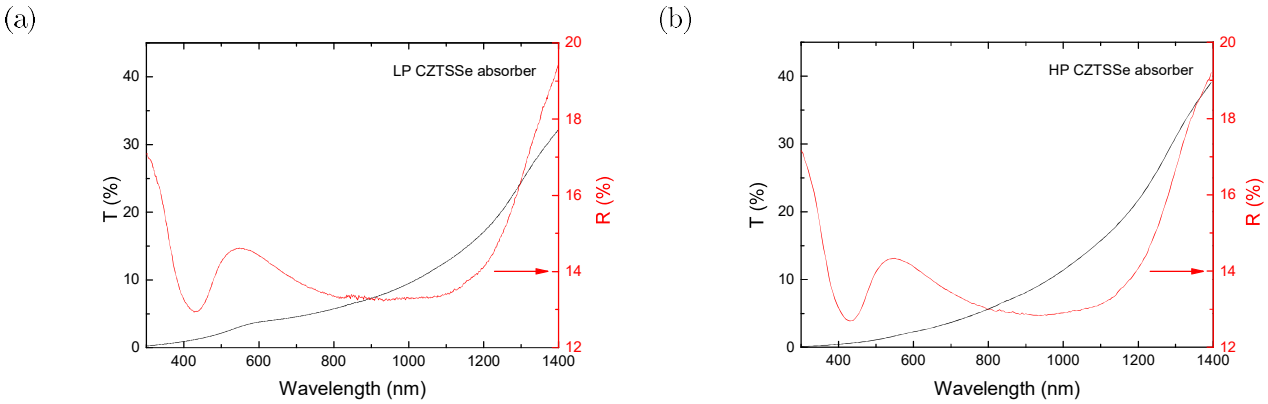

Figure S3: Transmission and absorption data of CZTSSe absorbers deposited on bare soda lime glass of (a) film LP and (b) film HP.